

## Article

# Photocatalytic H<sub>2</sub> Production on Au/TiO<sub>2</sub>: Effect of Au Photodeposition on Different TiO<sub>2</sub> Crystalline Phases

Stefano Andrea Balsamo, Salvatore Sciré , Marcello Condorelli  and Roberto Fiorenza \* 

Department of Chemical Sciences, University of Catania, Viale A. Doria 6, 95125 Catania, Italy; stefano.balsamo@phd.unict.it (S.A.B.); sscire@unict.it (S.S.); marcello.condorelli@unict.it (M.C.)

\* Correspondence: rfiorenza@unict.it; Tel.: +39-0957385012

**Abstract:** In this work, we investigated the role of the crystalline phases of titanium dioxide in the solar photocatalytic H<sub>2</sub> production by the reforming of glycerol, focusing the attention on the influence of photodeposited gold, as a metal co-catalyst, on TiO<sub>2</sub> surface. We correlated the photocatalytic activity of 1 wt% Au/TiO<sub>2</sub> in anatase, rutile, and brookite phases with the structural and optical properties determined by Raman spectroscopy, N<sub>2</sub> adsorption–desorption measurements, UV–vis Diffuse Reflectance Spectroscopy (UV–vis DRS), X-ray photoelectron spectroscopy (XPS), Photoluminescence spectroscopy (PL), and Dynamic Light scattering (DLS). The best results (2.55 mmol H<sub>2</sub> g<sub>cat</sub><sup>−1</sup> h<sup>−1</sup>) were obtained with anatase and gold photodeposited after 30 min of solar irradiation. The good performance of Au/TiO<sub>2</sub> in anatase form and the key importance of the strong interaction between gold and the peculiar crystalline phase of TiO<sub>2</sub> can be a starting point to efficiently improve photocatalysts design and experimental conditions, in order to favor a green hydrogen production through solar photocatalysis.

**Keywords:** hydrogen; photoreforming; titanium dioxide; glycerol; photocatalysis; gold



**Citation:** Balsamo, S.A.; Sciré, S.; Condorelli, M.; Fiorenza, R. Photocatalytic H<sub>2</sub> Production on Au/TiO<sub>2</sub>: Effect of Au Photodeposition on Different TiO<sub>2</sub> Crystalline Phases. *J* **2022**, *5*, 92–104. <https://doi.org/10.3390/j5010006>

Academic Editor: Rajender S. Varma

Received: 30 December 2021

Accepted: 19 January 2022

Published: 24 January 2022

**Publisher's Note:** MDPI stays neutral with regard to jurisdictional claims in published maps and institutional affiliations.



**Copyright:** © 2022 by the authors. Licensee MDPI, Basel, Switzerland. This article is an open access article distributed under the terms and conditions of the Creative Commons Attribution (CC BY) license (<https://creativecommons.org/licenses/by/4.0/>).

## 1. Introduction

Nowadays, the transition towards a more carbon-free society is a key point of technological and socio-economic progress. The environmental concerns related to the depletion of natural resources and atmospheric pollution require sustainable and green solutions. The development of new technologies based on renewables is the main road to drive the environmental transition. In this context, hydrogen is a promising energy carrier and can be the leading actor of the green innovation [1]. Unfortunately, until now, hydrogen has been mostly produced in a not sustainable way, namely, through the steam reforming of hydrocarbons, which requires fossil fuels and causes relevant CO<sub>2</sub> emissions [2].

In the last years, photocatalytic hydrogen production has received increasing attention due to its green potentiality. Since the pioneering work of Fujishima and Honda in the 1972 [3], scientific research has focused its attention on photocatalytic hydrogen production by water splitting or photoreforming of organic substrates [4,5]. This latter process is promising for a carbon-neutral vision, because the obtained CO<sub>2</sub> can be easily reconverted, even through the solar photocatalytic process, in bio-substrates [6]. Therefore, the sustainability of the process strongly depends on the choice of the organic substrates [7]. Many works reported the use of alcohols such methanol or ethanol or acids such as lactic or acetic acid, or also carbohydrates such as glucose as substrates [8–11].

Recently, the valorization of glycerol has attracted a growing interest, due to its large production as a by-product of biodiesel [12]. Furthermore, the photoreforming of glycerol (Reaction (1)) allows obtaining a high amount of hydrogen for each glycerol molecule [13,14].



The most used semiconductor material in photocatalysis is certainly titanium dioxide ( $\text{TiO}_2$ , titania). It has been largely investigated since the 1970s and is used in many applications [15–19]. It exists in three principal crystalline phases: anatase, rutile, and brookite. The first one is the most used in photocatalysis thanks to its chemico-physical properties [20]. Anatase has a tetragonal arrangement, is stable at room temperature, and is also the least dense among the three phases; this favors the mobility of charge carriers (photoelectrons and photoholes), which is an important parameter that explains its large use in photocatalysis [20]. Similar to the anatase, also the rutile phase has a tetragonal arrangement; however, it is more packed compared to anatase and thus generates a greater thermodynamic stability but also a greater density [21]. Finally, brookite is the least investigated crystalline form of  $\text{TiO}_2$  due to its low stability and the difficulty to obtain it as a pure phase. Brookite possesses an orthorhombic arrangement and an intermediate density amongst those of the three  $\text{TiO}_2$  crystalline forms ( $3.7 \text{ g/cm}^3$  for anatase,  $4.23 \text{ g/cm}^3$  for rutile, and  $4.12 \text{ g/cm}^3$  for brookite) [22].

The photocatalytic activity of  $\text{TiO}_2$  is strongly affected by two important issues: poor visible light absorption and high charge carrier recombination rate [23]. For these reasons, the presence of a co-catalyst, generally a noble metal, is usually required for photocatalytic hydrogen production. Many works reported that the presence of these metals on the surface of semiconductors promotes hydrogen evolution because they play the role of charges “accumulators”, being centers of electrons release necessary for proton reduction [24]. This leads to an improved charge carrier separation and to a higher photocatalytic activity.

Among the noble metals, gold also allows exploiting its surface plasmon resonance (SPR) effect that enhances visible light absorption and charges generation around the  $\text{TiO}_2$  surface [25–30]. Furthermore, as reported [31–33], the combination of a good interaction between gold and  $\text{TiO}_2$  and the Au SPR effect allowed obtaining a high photocatalytic  $\text{H}_2$  production under solar/visible irradiation, sometimes higher than that obtained with the other noble metal co-catalysts used for this reaction, such as Pt, Pd, or Ag. Finally, the chemico-physical properties of gold can be more easily tuned compared to those of the other noble metals, depending on the particular preparation method employed for gold deposition, i.e., deposition–precipitation, sol–gel, laser ablation, colloidal impregnation, etc. [31]. All these features make gold an ideal co-catalyst for  $\text{TiO}_2$  for the photoreforming and water splitting reactions.

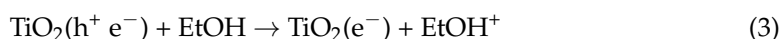
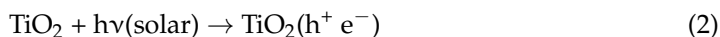
On the basis of the above considerations, in our work, we investigated hydrogen evolution through the photoreforming of glycerol using Au/ $\text{TiO}_2$  photocatalysts prepared by photodeposition of gold on the three crystalline phases of  $\text{TiO}_2$ . We explored in detail the modifications of the structural and optical properties due to gold photodeposition on the  $\text{TiO}_2$  phases and how these modifications affected the photocatalytic  $\text{H}_2$  evolution. The main novelty of the present work is the focus on the parameters that influence gold photodeposition on the different  $\text{TiO}_2$  polymorphs and their correlation with the photocatalytic activity in the photoreforming reaction. The solar photodeposition here proposed, can be considered an easy and sustainable route to prepare gold-based photocatalysts; it does not require peculiar thermal treatments or the use of expensive or toxic chemicals. Furthermore, it is also characterized by a high versatility: indeed, the same photoreactor can be used for both the materials’ synthesis and the photocatalytic tests.

## 2. Materials and Methods

### 2.1. Samples Preparation

Anatase, rutile, and brookite, titania were used as purchased (Sigma-Aldrich, Buchs, Switzerland). Tetrachloroauric acid ( $\text{HAuCl}_4$ , Merck KGAA, Darmstadt, Germany) was solubilized in water, and a  $5 \text{ g/L}$  solution was used as a precursor of gold co-catalysts. For gold deposition, the method described by Williams G., Seger B., and Kama P. [34] was slightly modified. In a typical procedure,  $0.2 \text{ g}$  of  $\text{TiO}_2$  powder was suspended in  $35 \text{ mL}$  of ethanol and put in a home-made jacketed batch Pyrex reactor, keeping the stirring at  $800 \text{ rpm}$  and the temperature at  $25 \text{ }^\circ\text{C}$ . Then, a stoichiometric amount of  $\text{HAuCl}_4$  (to obtain

a final Au content of 1 wt%) was added, and the suspension was purged with argon for 1 h in order to remove the oxygen inside the reactor. Then, a solar lamp (OSRAM Vitalux, OSRAM Opto Semiconductors GmbH, Leibniz, Regensburg Germany, 300 W, irradiance of 10.7 mW/cm<sup>2</sup>) was turned on for 30 min. This irradiation process generated the charge carriers (photoelectrons and holes) on TiO<sub>2</sub>. The holes were scavenged by ethanol, whereas the photoelectrons were able to reduce the Au<sup>3+</sup> ions. This process can be summarized with the following reactions:



Finally, the obtained powders were centrifuged and dried in an oven at 70 °C for 12 h. For comparison, bare titanium dioxide samples were used as purchased. Furthermore, for the most performing phase, the Au content and the time of irradiation in the photoreduction process were modified in order to find the best experimental conditions that promoted the final photocatalytic activity.

## 2.2. Samples Characterizations

The textural properties of the samples were analyzed by N<sub>2</sub> adsorption–desorption isotherms, carried out with a Micromeritics Tristar II Plus 3020 (Micromeritics Instrument Corp., Norcross, GA, USA) after an outgassing at 60 °C overnight. The Braunauer–Emmet–Teller (BET) theory, for the determination of the surface area, and the Barret–Joyner–Halenda (BJH) theory, for the determination of pore size distribution, were applied. The optical properties of the samples were investigated by UV–vis DRS (Diffuse Reflectance Spectroscopy), carried out with a JASCO V-670 (Jasco Europe S.R.L., Cremella, Italy) equipped with an integration sphere and using barium sulphate as a reflectance standard. The optical band gaps were estimated with the TAUC plot according with the Kubelka–Munk theory [35]. Dynamic Light Scattering (DLS) measures were carried out with a HORIBA (Horiba UK Limited, Kyoto Close, Moulton Park, Northampton, UK) Scientific nano particle analyzer SZ-100 in disposable PMMA cuvettes. Raman spectra were acquired by a WITec alpha 300 confocal Raman system (WITec Wissenschaftliche Instrument und Technologie GmbH, Ulm, Germany) with the experimental conditions described in the ref. [11]. X-ray photoelectron spectroscopy (XPS) was carried out with a K-Alpha X-ray photoelectron instrument (Thermo Fisher Scientific, Waltham, MA, USA), using the carbon 1s band at 284.9 eV (due to adventitious carbon) as a reference. Photoluminescence spectroscopy (PL) was performed with a Perkin Elmer LS45 luminescence Spectrometer (Perkin Elmer, Inc., Waltham, MA, USA).

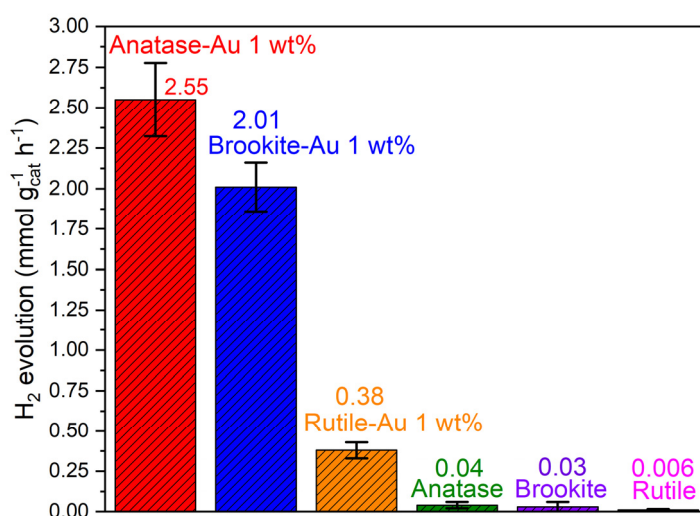
## 2.3. Photocatalytic Experiments

The photocatalytic tests were performed using the same Pyrex jacketed batch reactor and solar lamp employed for sample preparation. In these experiments, 50 mg of powder was suspended in 50 mL of a water–glycerol solution (45 mL and 5 mL respectively) under constant stirring at 800 rpm, and the temperature was kept at 35 °C. The suspension was purged 1 h with argon, and then the solar lamp was turned on for 4 h. The amount of hydrogen produced was evaluated with a gas chromatograph (Agilent 6890, Agilent Technologies, Santa Clara, CA, USA) equipped with a packed column (Carboxen 1000) and a TCD detector. Argon was used as the gas carrier. For H<sub>2</sub> quantification, a 0.5 mL aliquot of reaction gases was withdrawn using a syringe (Hamilton Gastight 1001, Hamilton, Bonaduz AG, Switzerland) and injected in the GC. For the reusability tests, after each run, the photocatalyst was centrifuged, washed with water, dried at room temperature, and then re-used.

### 3. Results and Discussion

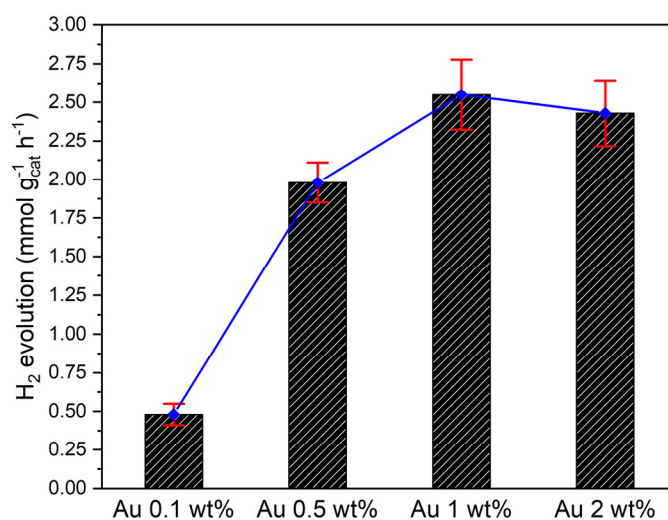
#### 3.1. Photocatalytic Activity

Figure 1 reports the photocatalytic activity data related to hydrogen evolution over the investigated TiO<sub>2</sub> and Au/TiO<sub>2</sub> samples. The best result was obtained with the Anatase–Au sample, which produced 2.55 mmol g<sub>cat</sub><sup>−1</sup> h<sup>−1</sup> of hydrogen after 4 h of solar light, followed by the Brookite–Au and Rutile–Au samples (2.01 and 0.38 mmol g<sub>cat</sub><sup>−1</sup> h<sup>−1</sup>, respectively). As expected, the bare oxides (anatase, brookite, and rutile) were almost inactive in the solar photoreforming reaction. Interestingly, for all the three TiO<sub>2</sub> phases, the addition of gold resulted in a significant increase of H<sub>2</sub> evolution (more than 60 times) compared to that achieved with the unmodified oxides. The interaction between gold and TiO<sub>2</sub> was better exploited when TiO<sub>2</sub> was in anatase form, whereas rutile TiO<sub>2</sub> gave the lowest photoactivity. This was in accordance with previous literature reports, pointing to the anatase form as the best supported phase for gold [36,37].



**Figure 1.** Hydrogen evolution on the investigated samples after 4 h of solar irradiation.

Figure 2 reports the trend of the photocatalytic activity as a function of the gold content on anatase. In this case, it is clear how, in our experimental conditions, the optimal amount of gold was 1 wt%.



**Figure 2.** Influence of the amount of gold deposited on anatase TiO<sub>2</sub> versus H<sub>2</sub> production.

This behavior can be rationalized considering that with photodeposition here used to prepare the Au/TiO<sub>2</sub> samples, an amount of gold higher than 1% can be detrimental, leading to an agglomeration of gold particles [38]. Moreover, a higher concentration of gold precursor resulted in a lower Au reduction efficiency in the photodeposition process [38]. However, considering the high cost of gold, the use of a relative low Au amount (0.5 or 1 wt%) can be highly positive in terms of the overall process sustainability.

Another key parameter of the photodeposition technique is the time of irradiation/deposition employed in the preparation of the supported Au photocatalysts. Table 1 summarizes the evolution of H<sub>2</sub> amounts on 1 wt% Au/TiO<sub>2</sub> anatase samples varying the solar irradiation times.

**Table 1.** Different irradiation–deposition times during the preparation of 1 wt% Au/TiO<sub>2</sub> anatase and their effect on the photocatalytic activity.

Irradiation Time [min]	H <sub>2</sub> Amount [mmol g <sub>cat</sub> <sup>-1</sup> h <sup>-1</sup> ]
15	2.24 ± 0.21
30	2.55 ± 0.24
45	2.14 ± 0.19
60	1.83 ± 0.16

It is possible to note that the best photocatalyst was obtained with an irradiation time of 30 min. Reasonably, lower times were not sufficient to reduce all the gold precursor, whereas higher times favored the agglomeration of gold particles.

Reusability tests were carried out to check the stability of the Anatase–Au 1 wt% sample, and the results are shown in Figure 3a,b. At the end of each run, the sample was centrifuged, dried at room temperature, and re-used without thermal treatments.

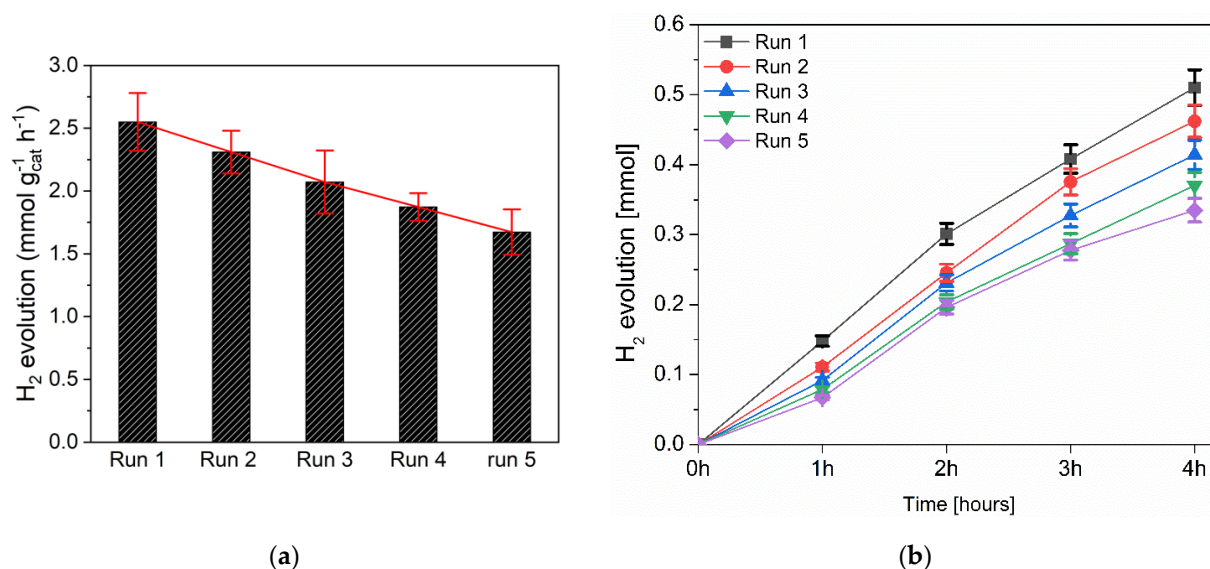


**Figure 3.** (a) Photocatalytic activity of Anatase–Au 1 wt% on five subsequent runs, (b) H<sub>2</sub> evolution in each hour of the stability tests.

The catalytic stability of Au/TiO<sub>2</sub> anatase was good until the third run; afterwards, there was a more substantial decrease of H<sub>2</sub> production, and in the fifth run, the photoactivity decreased by about 30% compared to the first run. The activity loss can be reasonably ascribed to the difficulty to recover all the powders after each consecutive test. However, a loss of efficiency due to the progressive aggregation of the gold particles on the surface of TiO<sub>2</sub> as a consequence of protracted solar irradiation cannot be excluded [39].

### 3.2. Samples Characterization

Figure 4 shows the UV–vis DRS spectra of the investigated samples (a) and the corresponding TAUC plots determined with the Kubelka–Munk function (b) to estimate the optical band gap of the samples.

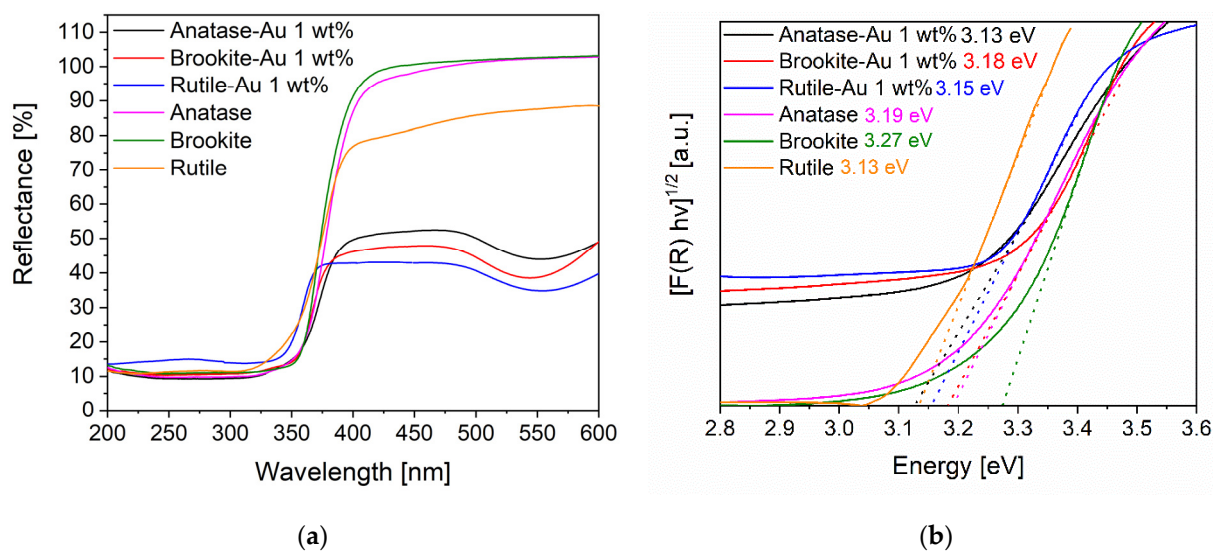


**Figure 4.** (a) UV–vis DRS measurements in R%, (b) Kubelka–Munk functions for the estimation of the optical band gap of the investigated samples.

No significant differences in the UV–vis DRS spectra were detected among the three  $\text{TiO}_2$  phases, whereas for all the gold-based samples, the presence of the surface plasmonic resonance (SPR) band of gold was evident at around 550 nm. This additional light absorption in the visible portion can be one of the crucial features that explain the significant enhancement of the photocatalytic activity due to the addition of gold on  $\text{TiO}_2$ . Furthermore, on anatase and brookite samples, the presence of gold determined a slight decrease of the band gap values (Figure 4b) compared to those of the corresponding unmodified oxides. On the contrary, the rutile-based Au sample showed similar values as bare rutile, indicating the smallest interaction between gold and  $\text{TiO}_2$  in the rutile phase, as also confirmed by the photocatalytic data. The SPR band was at 552 nm for the Au/ $\text{TiO}_2$  anatase, at 554 nm for the Au/ $\text{TiO}_2$  rutile, and at 542 nm for the Au/ $\text{TiO}_2$  brookite. This indicated that Au particle size was in the range 5–10 nm [37,40]. The correlation between the SPR band and gold size is influenced by the dielectric constant of the surrounding medium [37,40]; therefore, when gold is deposited on an oxide (such as  $\text{TiO}_2$ ), the wavelength of SPR is almost independent of Au particle size, contrary to what observed for unsupported gold (e.g., present as a colloidal solution). For the Au/ $\text{TiO}_2$  samples, the optical features of gold as well as the final photocatalytic  $\text{H}_2$  production were mainly related to the strength of the metal–support interaction.

The Raman spectra of the Au/ $\text{TiO}_2$  samples are reported in Figure 5. Gold deposition on titania surface did not change the crystalline structures of the bare oxides, being the spectra similar to those of pure anatase, rutile, and brookite, respectively (Figure S1).

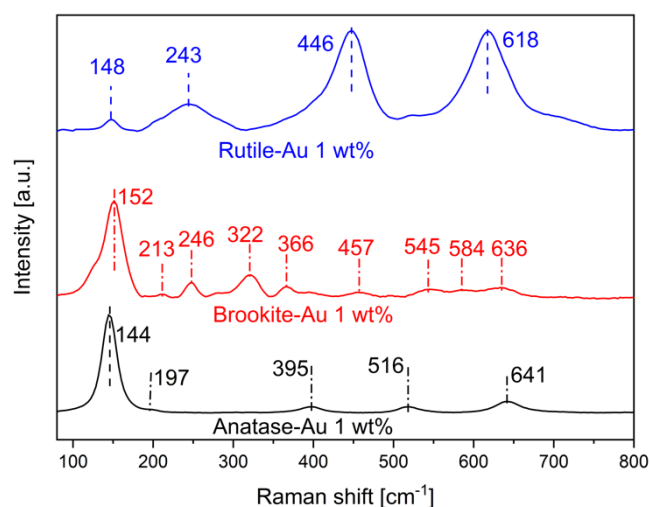


**Figure 5.** Raman spectra of the samples containing the gold particles.

In particular, for the anatase phase, we observed signals at  $144\text{ cm}^{-1}$ ,  $197\text{ cm}^{-1}$ ,  $395\text{ cm}^{-1}$ ,  $516\text{ cm}^{-1}$ , and  $641\text{ cm}^{-1}$ , related to  $E_g$ ,  $E_g$ ,  $B_{1g}$ ,  $A_{1g} + B_{1g}$ , and  $E_g$ , vibrational modes, respectively [41]. Regarding the rutile form, four different signals were detected at  $148\text{ cm}^{-1}$ ,  $446\text{ cm}^{-1}$ ,  $618\text{ cm}^{-1}$ , and  $243\text{ cm}^{-1}$ , assigned to the  $B_{1g}$ ,  $E_g$ ,  $A_{1g}$  modes and to a multi-phononic process, respectively [42]. Finally, a multitude of modes were detected in the brookite phase, assigned to  $A_{1g}$  ( $152\text{ cm}^{-1}$ ,  $246\text{ cm}^{-1}$ ,  $636\text{ cm}^{-1}$ ),  $B_{1g}$  ( $213\text{ cm}^{-1}$ ,  $322\text{ cm}^{-1}$ ),  $B_{2g}$  ( $366\text{ cm}^{-1}$ ,  $457\text{ cm}^{-1}$ ,  $584\text{ cm}^{-1}$ ), and  $B_{3g}$  ( $545\text{ cm}^{-1}$ ) [43]. The pure brookite phase was verified by the presence of the typical band at  $152\text{ cm}^{-1}$  and the absence of the vibrational mode at  $516$  and  $446\text{ cm}^{-1}$  of anatase and rutile, respectively.

The DLS (Dynamic Light Scattering) and  $N_2$  adsorption–desorption results for the investigated samples are reported in Table 2. Interestingly, a correlation existed between these features and the photocatalytic activity. In fact, the anatase phase showed the highest value of BET surface area ( $53\text{ m}^2/\text{g}$ ), followed by the brookite ( $46\text{ m}^2/\text{g}$ ) and finally by the rutile ( $38\text{ m}^2/\text{g}$ ) phases. In accordance, the DLS values ascribed to the hydrodynamic radius of the Au/TiO<sub>2</sub> samples followed a reverse trend compared to the surface area, being  $184\text{ nm}$ ,  $200\text{ nm}$ , and  $840\text{ nm}$ , for anatase, brookite, and rutile, respectively, similar to those of the bare oxides. As largely reported in the literature [44,45], a high surface area, in this case also favored by a small hydrodynamic radius, favors photocatalytic H<sub>2</sub> production, being this a surface reaction. This is another important feature that allowed obtaining the highest H<sub>2</sub> evolution on the Au/TiO<sub>2</sub> anatase sample. This sample, in fact, showed the highest surface area and the lowest hydrodynamic radius.

**Table 2.** Hydrodynamic radii, surface areas, and mean pore diameters of the investigated samples.

Samples	DLS <sup>1</sup> (nm)	S <sub>BET</sub> (m <sup>2</sup> /g)	d <sub>p</sub> <sup>2</sup> (nm)
Anatase	186	53;	20
Rutile	820	38	24
Brookite	210	46	24
Anatase–Au 1 wt%	184	55;	20
Rutile–Au 1 wt%	840	40;	25
Brookite–Au 1 wt%	200	49	24

<sup>1</sup> Hydrodynamic radius measured by Dynamic Light Scattering. <sup>2</sup> Average pore diameters determined with the Barret–Joyner–Halenda (BJH) method.

An interesting aspect is related to the BET surface area values after gold photodeposition, which slightly increased, probably thanks to the partial surface reduction of titania, as also observed previously, adopting the same photoreduction synthesis [46]. Finally, no par-

ticular variations were detected in the samples regarding the pore size. All photocatalysts were mesoporous, with pores in the range of 20–25 nm.

The surface properties of the Au/TiO<sub>2</sub> samples determined by x-ray photoelectron spectroscopy (XPS) are reported in Table 3 and Figure S2. For all samples, the Au 4f<sub>7/2</sub> and the Au 4f<sub>5/2</sub> spin-orbit components located at about 83.6 eV and 87.3 eV, respectively, were the typical signals of the Au<sup>0</sup> state [47], pointing to a complete photoreduction of the gold salt precursor on the surface of TiO<sub>2</sub> (see page 3, Reactions (2)–(4)). The measured surface content of gold was similar (0.84–0.86 wt%) to the nominal one (1 wt%), highlighting that all the deposited gold was on the surface of TiO<sub>2</sub>. The Ti 2p bands located at 458.8 eV and 464.8 eV for the anatase–Au sample were ascribed to Ti 2p<sub>3/2</sub> and Ti 2p<sub>1/2</sub>, respectively, and are the fingerprints of Ti<sup>4+</sup> in a tetragonal structure [48]. Consequently, the rutile–Au sample showed similar bands, whereas for the brookite–Au catalyst, these bands were slightly shifted (459.1 eV and 465.1 eV, respectively) due to the orthorhombic arrangement of brookite [49]. Finally, in the O 1s region, the band at about 530 eV and the component at about 532 eV were assigned to lattice oxygen in TiO<sub>2</sub> and to surface oxygen of hydroxyl species [50]. No significant differences were detected in the Ti and O regions considering the bare TiO<sub>2</sub> supports.

**Table 3.** XPS analysis of the Au-based samples.

Sample	Au 4f BE	Au Content (wt%)	Ti 2p BE	O 1s BE
Anatase–Au	83.6;87.3	0.86	458.8;464.8	529.9;531.6
Rutile–Au	83.6;87.3	0.84	458.9;464.9	530.3;532.6
Brookite–Au	83.6;87.3	0.84	459.1;460.0	530.8;531.9

### 3.3. Strong Metal Support Interaction (SMSI) between Gold and TiO<sub>2</sub>

The photodeposition of gold on TiO<sub>2</sub> gave the best results with the anatase phase, a gold content of 1 wt%, and a time of irradiation/deposition of 30 min. Under these experimental parameters, a satisfactory H<sub>2</sub> production was obtained, which was higher or comparable to those of the other Au/TiO<sub>2</sub>-based samples reported in the literature for the solar/visible photoreforming reaction (Table 4), although an accurate comparison is very difficult due to the various experimental conditions adopted by different research groups.

On the basis of the results of this work and of those reported in the literature [51–56], it is clear that the good interaction between gold and anatase favored H<sub>2</sub> evolution, and this is the most important feature that directly affects H<sub>2</sub> production, whereas the gold particle size played a minor role. This differentiates the catalytic behavior of gold-based samples in photocatalysis. Conversely, indeed, in thermocatalytic applications, the gold dimensions are crucial in order to have a good activity [57,58]. Moreover, the use of TiO<sub>2</sub> with a mixed phase (TiO<sub>2</sub> P25 is the most used “standard” sample, where however the anatase (80%) is preponderant with respect to the rutile (20%) phase) did not substantially improve H<sub>2</sub> evolution, being the values reported in the literature (Table 4) similar to or lower than those of the Au/TiO<sub>2</sub> anatase samples, as confirmed also in our experimental conditions, where the Au/TiO<sub>2</sub> P25 photocatalyst, prepared with the same experimental procedures reported in the Section 2.1 gave an H<sub>2</sub> production of 2.49 mmol g<sup>−1</sup> h<sup>−1</sup>, slightly lower than that of Au/TiO<sub>2</sub> anatase (2.55 mmol g<sup>−1</sup> h<sup>−1</sup>).

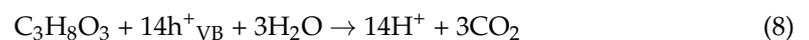
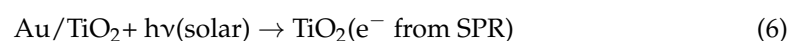
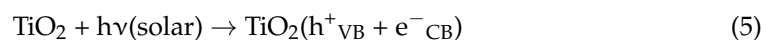
**Table 4.** Comparison of the solar/visible hydrogen evolution data from photoreforming on various Au/TiO<sub>2</sub>-based samples.

Sample	Gold Deposition Method and Au Size	H <sub>2</sub> Evolved <sup>1</sup>	Photocatalytic Conditions <sup>2</sup>	Ref.
1 wt% Au/TiO <sub>2</sub> anatase	Photodeposition, 5–10 nm	2.5	300 W solar lamp; 5 mL glycerol	this work
2 wt% Au/TiO <sub>2</sub> anatase	Deposition–precipitation, 6 nm	0.4	Natural sunlight; 5 mL ethanol	[52]
1 wt% Au/TiO <sub>2</sub> anatase	Sol-gel, 70 nm	2.0	500 W tungsten halogen lamp with a cut-off filter ( $\lambda > 400$ nm), 10 mL isopropanol	[53]
2 wt% Au/TiO <sub>2</sub> P25	Wet impregnation, 10 nm	2.7	300 W solar lamp; 10 mL methanol	[54]
0.94 wt% Au/TiO <sub>2</sub> P25	Sol immobilization, 9 nm	1.2	Vis. Light filtered 400–700 nm; 5 mL methanol	[55]
0.5 wt% Au/TiO <sub>2</sub> P25	Solid grinding, 23 nm	0.5	150 W Ceramic-Metal-Halide Lamp (solar light simulation), methanol 1% vol.	[56]

<sup>1</sup> Amount in mmol g<sub>cat</sub><sup>-1</sup> h<sup>-1</sup>; <sup>2</sup> irradiation source and sacrificial agent used in the photocatalytic experiments.

The here investigated photodeposition method led to a strong metal–support interaction (SMSI) with the anatase phase, with respect to the brookite and rutile phase. The higher hydrodynamic radius and the lower surface area of these latter crystalline phases compared to those of anatase did not favor an efficient gold deposition, thus explaining the lower activity. On the contrary, with the anatase, the combination of a high SMSI and an increased solar photoactivity, caused by the surface plasmon resonance effect of gold, resulted in a good H<sub>2</sub> production. Furthermore, as confirmed by the literature data (Table 4), the photocatalytic activity did not seem to be correlated with gold dimensions but appeared to be driven by the interaction between the gold co-catalyst and the TiO<sub>2</sub> crystalline phase.

Figure 6 shows the proposed reaction mechanism considering the obtained data. In particular, the UVA portion (in accordance with the obtained optical bandgap values) of solar irradiation led to the formation of holes (h<sup>+</sup>) and photoelectrons in the valence (VB) and in the conduction (CB) bands of TiO<sub>2</sub>, respectively, (Reaction (5)). The visible light portion of solar irradiation activated the surface plasmon resonance effect of gold deposited on the surface of TiO<sub>2</sub>, and allowed the injection of further electrons in the conduction band of TiO<sub>2</sub> (Reaction (6)). In this way, the photoelectrons and the electron coming from the Au SPR were able to efficiently reduce the proton from water (Reaction (7)), whereas the holes oxidized glycerol (hole scavengers), promoting the photoreforming (Reaction (8)) as well as the oxidation of water (Reaction (9)) [26,59]. In this way, charge carrier recombination (a common reason of photocatalysts deactivation) was strongly reduced, improving H<sub>2</sub> evolution.



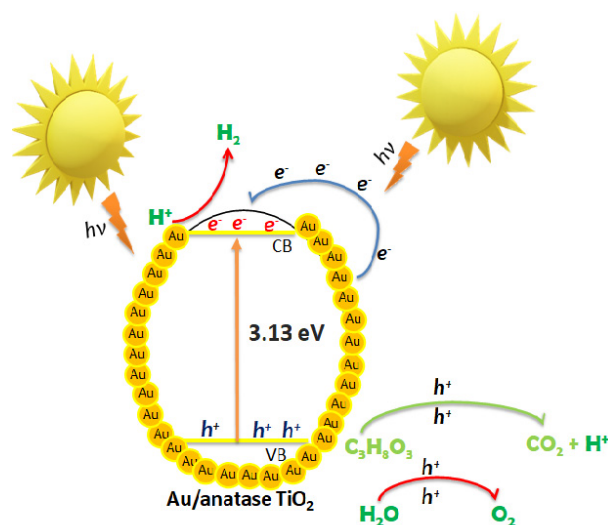


**Figure 6.** Proposed reaction mechanism.

The charge carrier separation was also improved by the presence of gold on  $\text{TiO}_2$ . This was verified by photoluminescence (PL) characterization, whose results are illustrated in the Figure 7. All samples showed four bands related to the band-to-band emission of  $\text{TiO}_2$  (388 nm), the self-trapped excitons localized on the surface of titania (420 nm), and the presence of oxygen vacancies and defects in  $\text{TiO}_2$  (485 and 525 nm) [60,61]. It is possible to note that the presence of gold led to a decrease of the intensity of these bands and that the Au/anatase  $\text{TiO}_2$  sample showed the lowest PL bands intensity. A lower PL intensity is generally related to a lower recombination rate of light-generated charge carriers [61], confirming that with the anatase form, the strong interaction with gold allowed a better improvement of charge carrier separation compared to Au/brookite  $\text{TiO}_2$  and Au/rutile photocatalysts. This is another key feature that clarifies the higher  $\text{H}_2$  production obtained with the gold/anatase sample with respect to the other investigated powders.

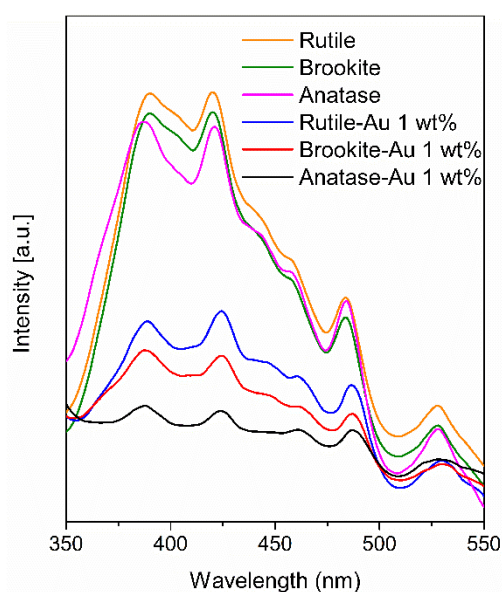


**Figure 7.** Photoluminescence spectra of the analyzed samples (excitation wavelength of 320 nm).

Finally, compared to the other preparation methods used for the preparation of gold/titania photocatalysts, such as deposition-precipitation, laser ablation, sol-gel, etc. [51,62], photodeposition certainly is an easy one-step preparation technique that avoids the addition of other chemicals and thermal treatments and that owns a promising versatility for possible

scale-up applications. In fact, the photoreactor can be used for both materials synthesis and photocatalytic tests. Furthermore, the use of glycerol as a sustainable organic substrate of photoreforming and the exploitation of solar light are promising aspects that will provide a high sustainability of the overall process for green hydrogen production.

#### 4. Conclusions

In this work, we investigated the performance in hydrogen evolution from solar photoreforming of glycerol of Au/TiO<sub>2</sub> samples prepared through the photodeposition of gold on different titanium dioxide phases. Very promising results were obtained using the anatase phase, with 2.55 mmol g<sub>cat</sub><sup>-1</sup> h<sup>-1</sup> of evolved hydrogen. The rutile phase showed the lowest photocatalytic activity due to its biggest hydrodynamic radius and lowest surface area compared to the anatase and brookite phases, which inhibited the interaction with gold. The best amount of gold was 1 wt% on TiO<sub>2</sub> anatase. The solar photodeposition method is promising for gold deposition on a semiconductor surface avoiding expensive procedures and thermal treatments. Finally, the use of solar light efficiently activated the gold surface plasmon resonance effect, with the double positive effect of favoring the interaction with anatase and the absorption of solar light, boosting up H<sub>2</sub> production.

**Supplementary Materials:** The following are available online at <https://www.mdpi.com/article/10.3390/j5010006/s1>, Figure S1: Raman spectra of bare anatase, rutile, and brookite TiO<sub>2</sub>; Figure S2: XPS spectra of the analyzed samples.

**Author Contributions:** Conceptualization, S.A.B. and R.F.; investigation, S.A.B., R.F. and M.C.; writing—original draft preparation, S.A.B.; writing—review and editing, R.F. and S.S.; supervision, R.F. and S.S. All authors have read and agreed to the published version of the manuscript.

**Funding:** This research received no external funding.

**Institutional Review Board Statement:** Not applicable.

**Informed Consent Statement:** Not applicable.

**Data Availability Statement:** The data presented in this study are available on request from the corresponding author.

**Acknowledgments:** R.F. thanks the PON “AIM” of the European Social Found (ESF) (CUP:E66C18001220005), S.S. thanks the University of Catania (Piano della ricerca 2020–2022) for the support to this research work.

**Conflicts of Interest:** The authors declare no conflict of interest.

#### References

1. Armaroli, N.; Balzani, V. The Future of Energy Supply: Challenges and Opportunities. *Angew. Chem. Int. Ed.* **2007**, *46*, 52–66. [CrossRef]
2. Holladay, J.D.; Hu, J.; King, D.L.; Wang, Y. An overview of hydrogen production technologies. *Catal. Today* **2009**, *139*, 244–260. [CrossRef]
3. Fujishima, A.; Honda, K. Electrochemical Photolysis of Water at a Semiconductor Electrode. *Nature* **1972**, *238*, 37–38. [CrossRef] [PubMed]
4. Yadav, A.A.; Hunge, Y.M.; Kang, S.-W. Porous nanoplate-like tungsten trioxide/reduced graphene oxide catalyst for sonocatalytic degradation and photocatalytic hydrogen production. *Surf. Interfaces* **2021**, *24*, 101075. [CrossRef]
5. Hunge, Y.M.; Yadav, A.A.; Mathe, V.L. Photocatalytic hydrogen production using TiO<sub>2</sub> nanogranules prepared by hydrothermal route. *Chem. Phys. Lett.* **2019**, *731*, 136582. [CrossRef]
6. Bellardita, M.; García-López, E.I.; Marci, G.; Nasillo, G.; Palmisano, L. Photocatalytic Solar Light H<sub>2</sub> Production by Aqueous Glucose Reforming. *Eur. J. Inorg. Chem.* **2018**, *2018*, 4522–4532. [CrossRef]
7. Zinoviev, S.; Müller-Langer, F.; Das, P.; Bertero, N.; Fornasiero, P.; Kaltschmitt, M.; Centi, G.; Miertus, S. Next-Generation Biofuels: Survey of Emerging Technologies and Sustainability Issues. *ChemSusChem* **2010**, *3*, 1106–1133. [CrossRef]
8. Bahadori, E.; Ramis, G.; Zanardo, D.; Menegazzo, F.; Signoreto, M.; Gazzoli, D.; Pietrogioacomi, D.; Di Michele, A.; Rossetti, I. Photoreforming of Glucose over CuO/TiO<sub>2</sub>. *Catalysts* **2020**, *10*, 477. [CrossRef]
9. Lakhera, S.K.; Rajan, A.; Rugma, T.P.; Bernaurdshaw, N. A review on particulate photocatalytic hydrogen production system: Progress made in achieving high energy conversion efficiency and key challenges ahead. *Renew. Sustain. Energy Rev.* **2021**, *152*, 111694. [CrossRef]
10. Huang, H.; Feng, J.; Zhang, S.; Zhang, H.; Wang, X.; Yu, T.; Chen, C.; Yi, Z.; Ye, J.; Li, Z.; et al. Molecular-level understanding of the deactivation pathways during methanol photo-reforming on Pt-decorated TiO<sub>2</sub>. *Appl. Catal. B Environ.* **2020**, *272*, 118980. [CrossRef]

11. Fiorenza, R.; Balsamo, S.A.; Condorelli, M.; D'Urso, L.; Compagnini, G.; Scirè, S. Solar photocatalytic H<sub>2</sub> production over CeO<sub>2</sub>-based catalysts: Influence of chemical and structural modifications. *Catal. Today* **2021**, *380*, 187–198. [[CrossRef](#)]
12. Chilakamarry, C.R.; Mimi Sakinah, A.M.; Zularisam, A.W.; Pandey, A.; Vo, D.-V.N. Technological perspectives for utilisation of waste glycerol for the production of biofuels: A review. *Environ. Technol. Innov.* **2021**, *24*, 101902. [[CrossRef](#)]
13. Hidalgo-Carrillo, J.; Martín-Gómez, J.; Morales, J.; Espejo, J.C.; Urbano, F.J.; Marinas, A. Hydrogen Photo-Production from Glycerol Using Nickel-Doped TiO<sub>2</sub> Catalysts: Effect of Catalyst Pre-Treatment. *Energies* **2019**, *12*, 3351. [[CrossRef](#)]
14. Christoforidis, K.C.; Fornasiero, P. Photocatalytic Hydrogen Production: A Rift into the Future Energy Supply. *ChemCatChem* **2017**, *9*, 1523–1544. [[CrossRef](#)]
15. Padmanabhan, N.T.; John, H. Titanium dioxide based self-cleaning smart surfaces: A short review. *J. Environ. Chem. Eng.* **2020**, *8*, 104211. [[CrossRef](#)]
16. Li, R.; Li, T.; Zhou, Q. Impact of Titanium Dioxide (TiO<sub>2</sub>) Modification on Its Application to Pollution Treatment—A Review. *Catalysts* **2020**, *10*, 804. [[CrossRef](#)]
17. Gopinath, K.P.; Madhav, N.V.; Krishnan, A.; Malolan, R.; Rangarajan, G. Present applications of titanium dioxide for the photocatalytic removal of pollutants from water: A review. *J. Environ. Manag.* **2020**, *270*, 110906. [[CrossRef](#)]
18. Nabi, I.; Bacha, A.-U.-R.; Ahmad, F.; Zhang, L. Application of titanium dioxide for the photocatalytic degradation of macro- and micro-plastics: A review. *J. Environ. Chem. Eng.* **2021**, *9*, 105964. [[CrossRef](#)]
19. Fiorenza, R.; Scirè, S.; D'Urso, L.; Compagnini, G.; Bellardita, M.; Palmisano, L. Efficient H<sub>2</sub> production by photocatalytic water splitting under UV or solar light over variously modified TiO<sub>2</sub>-based catalysts. *Int. J. Hydrogen Energy* **2019**, *44*, 14796–14807. [[CrossRef](#)]
20. Labat, F.; Baranek, P.; Adamo, C. Structural and Electronic Properties of Selected Rutile and Anatase TiO<sub>2</sub> Surfaces: An ab Initio Investigation. *J. Chem. Theory Comput.* **2008**, *4*, 341–352. [[CrossRef](#)]
21. Sikora, R. Ab initio study of phonons in the rutile structure of TiO<sub>2</sub>. *J. Phys. Chem. Solids* **2005**, *66*, 1069–1073. [[CrossRef](#)]
22. Di Paola, A.; Bellardita, M.; Palmisano, L. Brookite, the Least Known TiO<sub>2</sub> Photocatalyst. *Catalysts* **2013**, *3*, 36–73. [[CrossRef](#)]
23. Fujishima, A.; Rao, T.N.; Tryk, D.A. Titanium dioxide photocatalysis. *J. Photochem. Photobiol. C Photochem. Rev.* **2000**, *1*, 1–21. [[CrossRef](#)]
24. Linsebigler, A.L.; Lu, G.; Yates, J.T. Photocatalysis on TiO<sub>2</sub> Surfaces: Principles, Mechanisms, and Selected Results. *Chem. Rev.* **1995**, *95*, 735–758. [[CrossRef](#)]
25. Wibowo, D.; Muzakkar, M.Z.; Saad, S.K.M.; Mustapa, F.; Maulidiyah, M.; Nurdin, M.; Umar, A.A. Enhanced visible light-driven photocatalytic degradation supported by Au-TiO<sub>2</sub> coral-needle nanoparticles. *J. Photochem. Photobiol. A Chem.* **2020**, *398*, 112589. [[CrossRef](#)]
26. Fiorenza, R.; Bellardita, M.; D'Urso, L.; Compagnini, G.; Palmisano, L.; Scirè, S. Au/TiO<sub>2</sub>-CeO<sub>2</sub> catalysts for photocatalytic water splitting and VOCs oxidation reactions. *Catalysts* **2016**, *6*, 121. [[CrossRef](#)]
27. Greco, E.; Balsamo, S.A.; Maccarrone, G.; Mello, D.; Ciliberto, E.; Shang, J.; Zhu, T. Gold-core lithium-doped titania shell nanostructures for plasmon-enhanced visible light harvesting with photocatalytic activity. *J. Nanoparticle Res.* **2020**, *22*, 164. [[CrossRef](#)]
28. Mohite, V.S.; Mahadik, M.A.; Kumbhar, S.S.; Hunge, Y.M.; Kim, J.H.; Moholkar, A.V.; Rajpure, K.Y.; Bhosale, C.H. Photoelectrocatalytic degradation of benzoic acid using Au doped TiO<sub>2</sub> thin films. *J. Photochem. Photobiol. B Biol.* **2015**, *142*, 204–211. [[CrossRef](#)]
29. Mohazzab, B.F.; Jaleh, B.; Nasrollahzadeh, M.; Issaabadi, Z.; Varma, R.S. Laser ablation-assisted synthesis of GO/TiO<sub>2</sub>/Au nanocomposite: Applications in K<sub>3</sub>[Fe(CN)<sub>6</sub>] and Nigrosin reduction. *Mol. Catal.* **2019**, *473*, 110401. [[CrossRef](#)]
30. Fadaee Takmil, N.; Jaleh, B.; Feizi Mohazzab, B.; Khazalpour, S.; Rostami-Vartooni, A.; Hong Chuong Nguyen, T.; Cuong Nguyen, X.; Varma, R.S. Hydrogen production by electrochemical reaction using waste zeolite boosted with Titania and Au nanoparticles. *Inorg. Chem. Commun.* **2021**, *133*, 108891. [[CrossRef](#)]
31. Kumaravel, V.; Mathew, S.; Bartlett, J.; Pillai, S.C. Photocatalytic hydrogen production using metal doped TiO<sub>2</sub>: A review of recent advances. *Appl. Catal. B Environ.* **2019**, *244*, 1021–1064. [[CrossRef](#)]
32. Huang, L.; Liu, X.; Wu, H.; Wang, X.; Wu, H.; Li, R.; Shi, L.; Li, C. Surface state modulation for size-controllable photodeposition of noble metal nanoparticles on semiconductors. *J. Mater. Chem. A* **2020**, *8*, 21094–21102. [[CrossRef](#)]
33. Lettieri, S.; Pavone, M.; Fioravanti, A.; Santamaria Amato, L.; Maddalena, P. Charge Carrier Processes and Optical Properties in TiO<sub>2</sub> and TiO<sub>2</sub>-Based Heterojunction Photocatalysts: A Review. *Materials* **2021**, *14*, 1645. [[CrossRef](#)] [[PubMed](#)]
34. Williams, G.; Seger, B.; Kamat, P.V. TiO<sub>2</sub>-Graphene Nanocomposites. UV-Assisted Photocatalytic Reduction of Graphene Oxide. *ACS Nano* **2008**, *2*, 1487–1491. [[CrossRef](#)]
35. Makuła, P.; Pacia, M.; Macyk, W. How To Correctly Determine the Band Gap Energy of Modified Semiconductor Photocatalysts Based on UV-Vis Spectra. *J. Phys. Chem. Lett.* **2018**, *9*, 6814–6817. [[CrossRef](#)]
36. Martins, P.; Kappert, S.; Nga Le, H.; Sebastian, V.; Kühn, K.; Alves, M.; Pereira, L.; Cuniberti, G.; Melle-Franco, M.; Lanceros-Méndez, S. Enhanced Photocatalytic Activity of Au/TiO<sub>2</sub> Nanoparticles against Ciprofloxacin. *Catalysts* **2020**, *10*, 234. [[CrossRef](#)]
37. Chen, W.-T.; Chan, A.; Al-Azri, Z.H.N.; Dosado, A.G.; Nadeem, M.A.; Sun-Waterhouse, D.; Idriss, H.; Waterhouse, G.I.N. Effect of TiO<sub>2</sub> polymorph and alcohol sacrificial agent on the activity of Au/TiO<sub>2</sub> photocatalysts for H<sub>2</sub> production in alcohol–water mixtures. *J. Catal.* **2015**, *329*, 499–513. [[CrossRef](#)]
38. Kimling, J.; Maier, M.; Okenve, B.; Kotaidis, V.; Ballot, H.; Plech, A. Turkevich Method for Gold Nanoparticle Synthesis Revisited. *J. Phys. Chem. B* **2006**, *110*, 15700–15707. [[CrossRef](#)]
39. Zhang, D.-F.; Li, S.; Xu, Q.-H.; Cao, Y. Aggregation-Induced Plasmon Coupling-Enhanced One- and Two-Photon Excitation Fluorescence by Silver Nanoparticles. *Langmuir* **2020**, *36*, 4721–4727. [[CrossRef](#)]
40. Kowalska, E.; Mahaney, O.O.P.; Abe, R.; Ohtani, B. Visible-light-induced photocatalysis through surface plasmon excitation of gold on titania surfaces. *Phys. Chem. Chem. Phys.* **2010**, *12*, 2344. [[CrossRef](#)]

41. Ohsaka, T.; Izumi, F.; Fujiki, Y. Raman spectrum of anatase, TiO<sub>2</sub>. *J. Raman Spectrosc.* **1978**, *7*, 321–324. [[CrossRef](#)]
42. Challagulla, S.; Tarafder, K.; Ganesan, R.; Roy, S. Structure sensitive photocatalytic reduction of nitroarenes over TiO<sub>2</sub>. *Sci. Rep.* **2017**, *7*, 8783. [[CrossRef](#)] [[PubMed](#)]
43. Xu, J.; Li, K.; Wu, S.; Shi, W.; Peng, T. Preparation of brookite titania quasi nanocubes and their application in dye-sensitized solar cells. *J. Mater. Chem. A* **2015**, *3*, 7453–7462. [[CrossRef](#)]
44. Liu, B.; Liu, L.-M.; Lang, X.-F.; Wang, H.-Y.; Lou, X.W.D.; Aydil, E.S. Doping high-surface-area mesoporous TiO<sub>2</sub> microspheres with carbonate for visible light hydrogen production. *Energy Environ. Sci.* **2014**, *7*, 2592. [[CrossRef](#)]
45. Schwarze, M.; Klingbeil, C.; Do, H.U.; Kutorglo, E.M.; Parapat, R.Y.; Tasbihi, M. Highly Active TiO<sub>2</sub> Photocatalysts for Hydrogen Production through a Combination of Commercial TiO<sub>2</sub> Material Selection and Platinum Co-Catalyst Deposition Using a Colloidal Approach with Green Reductants. *Catalysts* **2021**, *11*, 1027. [[CrossRef](#)]
46. Balsamo, S.A.; Fiorenza, R.; Condorelli, M.; Pecoraro, R.; Brundo, M.V.; Lo Presti, F.; Sciré, S. One-Pot Synthesis of TiO<sub>2</sub>-rGO Photocatalysts for the Degradation of Groundwater Pollutants. *Materials* **2021**, *14*, 5938. [[CrossRef](#)]
47. Casaletto, M.P.; Longo, A.; Martorana, A.; Prestianni, A.; Venezia, A.M. XPS study of supported gold catalysts: The role of Au<sup>0</sup> and Au<sup>+δ</sup> species as active sites. *Surf. Interface Anal.* **2006**, *38*, 215–218. [[CrossRef](#)]
48. Bian, Z.; Zhu, J.; Wang, S.; Cao, Y.; Qian, X.; Li, H. Self-Assembly of Active Bi<sub>2</sub>O<sub>3</sub>/TiO<sub>2</sub> Visible Photocatalyst with Ordered Mesoporous Structure and Highly Crystallized Anatase. *J. Phys. Chem. C* **2008**, *112*, 6258–6262. [[CrossRef](#)]
49. Fiorenza, R.; Bellardita, M.; Balsamo, S.A.; Spitaleri, L.; Gulino, A.; Condorelli, M.; D'Urso, L.; Sciré, S.; Palmisano, L. A solar photothermocatalytic approach for the CO<sub>2</sub> conversion: Investigation of different synergisms on CoO-CuO/brookite TiO<sub>2</sub>-CeO<sub>2</sub> catalysts. *Chem. Eng. J.* **2022**, *428*, 131249. [[CrossRef](#)]
50. Zhu, J.; Yang, J.; Bian, Z.-F.; Ren, J.; Liu, Y.-M.; Cao, Y.; Li, H.-X.; He, H.-Y.; Fan, K.-N. Nanocrystalline anatase TiO<sub>2</sub> photocatalysts prepared via a facile low temperature nonhydrolytic sol-gel reaction of TiCl<sub>4</sub> and benzyl alcohol. *Appl. Catal. B Environ.* **2007**, *76*, 82–91. [[CrossRef](#)]
51. Gupta, B.; Melvin, A.A.; Matthews, T.; Dash, S.; Tyagi, A.K. TiO<sub>2</sub> modification by gold (Au) for photocatalytic hydrogen (H<sub>2</sub>) production. *Renew. Sustain. Energy Rev.* **2016**, *58*, 1366–1375. [[CrossRef](#)]
52. Waterhouse, G.I.N.; Wahab, A.K.; Al-Oufi, M.; Jovic, V.; Anjum, D.H.; Sun-Waterhouse, D.; Llorca, J.; Idriss, H. Hydrogen production by Tuning the Photonic Band Gap with the Electronic Band Gap of TiO<sub>2</sub>. *Sci. Rep.* **2013**, *3*, 2849. [[CrossRef](#)] [[PubMed](#)]
53. Seh, Z.W.; Liu, S.; Low, M.; Zhang, S.Y.; Liu, Z.; Mlayah, A.; Han, M.Y. Janus Au-TiO<sub>2</sub> photocatalysts with strong localization of plasmonic near-fields for efficient visible-light hydrogen generation. *Adv. Mater.* **2012**, *24*, 2310–2314. [[CrossRef](#)] [[PubMed](#)]
54. Liu, R.; Fang, S.-Y.; Dong, C.-D.; Tsai, K.-C.; Yang, W.-D. Enhancing hydrogen evolution of water splitting under solar spectra using Au/TiO<sub>2</sub> heterojunction photocatalysts. *Int. J. Hydrogen Energy* **2021**, *46*, 28462–28473. [[CrossRef](#)]
55. Priebe, J.B.; Radnik, J.; Lennox, A.J.J.; Pohl, M.-M.; Karnahl, M.; Hollmann, D.; Grabow, K.; Bentrup, U.; Junge, H.; Beller, M.; et al. Solar Hydrogen Production by Plasmonic Au-TiO<sub>2</sub> Catalysts: Impact of Synthesis Protocol and TiO<sub>2</sub> Phase on Charge Transfer Efficiency and H<sub>2</sub> Evolution Rates. *ACS Catal.* **2015**, *5*, 2137–2148. [[CrossRef](#)]
56. Marchal, C.; Piquet, A.; Behr, M.; Cottineau, T.; Papaefthimiou, V.; Keller, V.; Caps, V. Activation of solid grinding-derived Au/TiO<sub>2</sub> photocatalysts for solar H<sub>2</sub> production from water-methanol mixtures with low alcohol content. *J. Catal.* **2017**, *352*, 22–34. [[CrossRef](#)]
57. Fiorenza, R. Bimetallic Catalysts for Volatile Organic Compound Oxidation. *Catalysts* **2020**, *10*, 661. [[CrossRef](#)]
58. Ishida, T.; Murayama, T.; Taketoshi, A.; Haruta, M. Importance of Size and Contact Structure of Gold Nanoparticles for the Genesis of Unique Catalytic Processes. *Chem. Rev.* **2020**, *120*, 464–525. [[CrossRef](#)]
59. Panagiotopoulou, P.; Karamerou, E.E.; Kondarides, D.I. Kinetics and mechanism of glycerol photo-oxidation and photo-reforming reactions in aqueous TiO<sub>2</sub> and Pt/TiO<sub>2</sub> suspensions. *Catal. Today* **2013**, *209*, 91–98. [[CrossRef](#)]
60. Serpone, N.; Lawless, D.; Khairutdinov, R. Size Effects on the Photophysical Properties of Colloidal Anatase TiO<sub>2</sub> Particles: Size Quantization versus Direct Transitions in This Indirect Semiconductor? *J. Phys. Chem.* **1995**, *99*, 16646–16654. [[CrossRef](#)]
61. Chen, Y.; Wang, Y.; Li, W.; Yang, Q.; Hou, Q.; Wei, L.; Liu, L.; Huang, F.; Ju, M. Enhancement of photocatalytic performance with the use of noble-metal-decorated TiO<sub>2</sub> nanocrystals as highly active catalysts for aerobic oxidation under visible-light irradiation. *Appl. Catal. B Environ.* **2017**, *210*, 352–367. [[CrossRef](#)]
62. Ayati, A.; Ahmadpour, A.; Bamoharram, F.F.; Tanhaei, B.; Mänttari, M.; Sillanpää, M. A review on catalytic applications of Au/TiO<sub>2</sub> nanoparticles in the removal of water pollutant. *Chemosphere* **2014**, *107*, 163–174. [[CrossRef](#)] [[PubMed](#)]